Experimental Demonstration of 224 Gbit/s PM-PAM4 IM/DD Transmission System using TFLN Polarization Controller

Juntao Cao, Haiqiang Wei, Weibing Chen, Hongwei Zhang, Ao Cui, Xingjie Li, Chao Lu *Fellow, Optica*, Alan Pak Tao Lau *Fellow, Optica*, Changjian Guo, Kangping Zhong

***Abstract*—In this paper, we experimentally demonstrated 224 Gbit/s polarization-multiplexed (PM) PAM4 intensity modulation and direct detection (IM/DD) transmission system using a thin-film Lithium Niobate (TFLN) polarization controller. We proposed and implemented a pilot-tone-assisted and calibration-free polarization tracking algorithm in an FPGA, achieved a record convergence time of 0.2 ms and polarization tracking speed of 2 krad/s for PM-IM/DD systems. The proposed scheme enables stable dual-polarization demultiplexing under fast polarization perturbations and represents a step towards practical high-speed, low-complexity PM-IM/DD systems with robust polarization tracking performance.**

***Index Terms*—Optical fiber communication, polarization multiplexing, IM/DD, active polarization tracking, TFLN.**

I. Introduction

With the rapid advancement of artificial intelligence (AI), 5G networks, cloud computing, and virtual reality, the demand for high-speed optical communication systems has reached unprecedented levels [1], [2]. In particular, AI's increasing computational power is driving massive traffic between data centers, further amplifying the need for efficient and scalable optical interconnects [3], [4]. This increase in demand calls for more advanced and high-speed optical interfaces, especially in short-reach optical communication scenarios where traditional solutions face limitations. Intensity modulation and direct detection (IM/DD) systems have been the dominant choice in short-reach inter- and intra-data center connections due to their low cost and power efficiency. Recently, single wavelength 200 Gbit/s and even 400 Gbit/s IM/DD systems are demonstrated by using ultra-high bandwidth modulators and receivers [5], [6]. However, it is challenging to increase the transmission capacity further as it is difficult to further push the bandwidth of optoelectronic devices in a cost and power-efficient manner. In addition, IM/DD transmissions are limited by low receiver sensitivity and power degradation caused by chromatic dispersion [7].

Inspired by the benefits of coherent detection, polarization-multiplexed (PM), which is widely used in long-haul coherent communications, is another degree of freedom to double the transmission rate of IM/DD systems. Polarization tracking is digitally realized using the full optical field information [8]. In this connection, various approaches have been reported to achieve active polarization tracking for PM-IM/DD systems. Nespola et al. demonstrated a PM-PAM transmission system by using a multistage Mach-Zehnder interferometer (MZI)-based polarization controller in a silicon photonic platform [9], [10]. A feedback control loop based on pilot-tone signals was used for real-time active polarization tracking. Polarization tracking rate is limited to around 100 rad/s due to constraints from the low response speed of the thermal tuning mechanism in the silicon photonic chip. This limits its potential to be deployed in a practical system with rapid polarization fluctuations. In addition to MZI-based architectures. Chan et al. proposed a compact form factor polarization demultiplexer based on a micro-ring resonator for PM-IM/DD systems [11]. However, the performance was only demonstrated in a static transmission system and no further study was undertaken in a system with dynamic polarization rotations. Wu et al. reported a fully integrated dual-polarization silicon photonic transceiver with automated polarization control [12]. A marker-tone and polarization-assisted tracking method was implemented in an MZI polarization control chip, and a low tracking speed of 0.02π rad/s was achieved due to the inherently low thermal response speed. Building on similar architectures, Zhao et al. developed PM-IM/DD system using a multistage MZI-based polarization controller guided by a real-time polarization state monitoring [13], [14], [15]. A tracking speed of 100 rad/s was demonstrated in a 400 Gbit/s PM-IM/DD system. However, the tracking rate cannot be further improved as it is still based on thermal tuning mechanisms. Fast polarization tracking is essential for deploying PM-IM/DD in practical applications.

In this connection, lithium Niobate (LiNbO3) has been used for fast polarization maintaining and signal modulation for a few decades [16], [17], [18], but bulk LiNbO3 requires high driving voltage and has a large form factor. Recently, thin-film Lithium Niobate (TFLN) has attracted more attention due to its high bandwidth, low driving voltage, and potential for high-density integration [19], [20], [21]. Using specifically engineered structural designs, polarization controllers based on TFLN platforms have been successfully

Manuscript received 2 July 2025; revised 28 August 2025; accepted 09 September 2025. Date of publication xx xx 2025; date of current version xx xx 2025. This work is supported by National Key Research and Development Program of China (2024YFB2908001, 2024YFB2807703), The Hong Kong Government General Research Fund (PolyU25227524, PolyU15225423, C5078-24G), ITF PRP/037/24FX, Hong Kong Polytechnic University (1-BEA9, G-SB1P, 1-CD8L,1-CDM9), Shenzhen Research Insititue of Hong Kong Polytechnic University (J2024A002). (Corresponding authors: Kangping Zhong, Alan Pak Tao Lau email:kangping.zhong@polyu.edu.hk;alan.pt.lau@polyu.edu.hk).

Juntao Cao, Haiqiang Wei, Chao Lu, Alan Pak Tao Lau, and Kangping Zhong are with the Photonics Research Institute, Department of Electrical and Electronic Engineering, The Hong Kong Polytechnic University, Hong Kong SAR, China (emails:juntao18.cao@connect.polyu.hk; haiqiang3.wei@connect.polyu.hk;enluchao@polyu.edu.hk;alan.pt.lau@polyu.edu.hk;kangping.zhong@polyu.edu.hk). Weibing Chen, Hongwei Zhang, Ao Cui, Xingjie Li, Changjian Guo are with South China Normal University, Guangzhou, China (email: weibinchen@m.scnu.edu.cn; 1344492779@qq.com;ccui_ao7@163.com;2022024062@m.scnu.edu.cn; changjianguo@m.scnu.edu.cn).

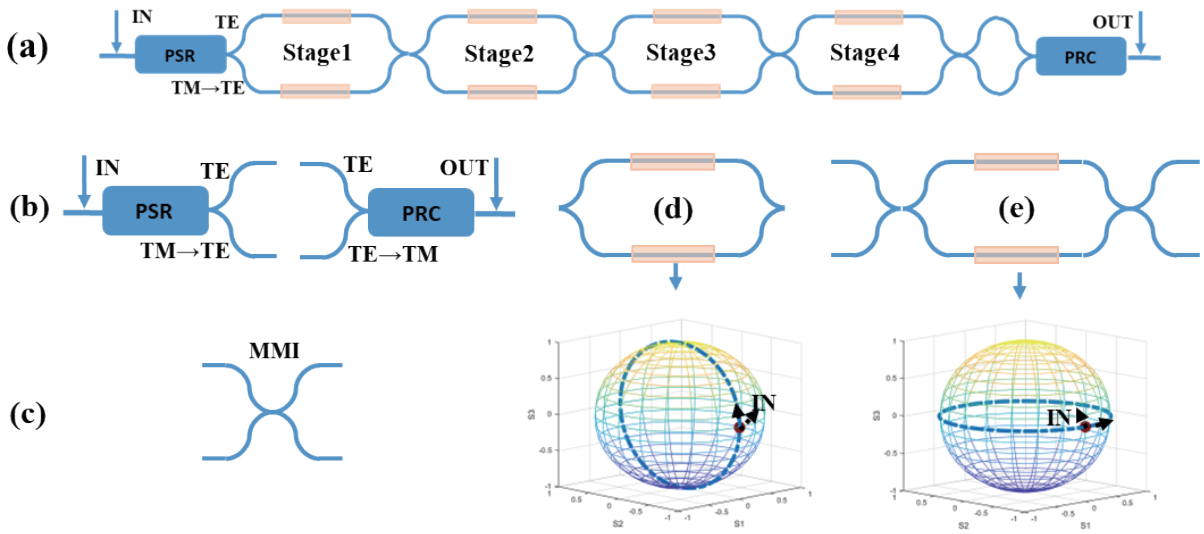

Fig. 1. The basic units of the polarization controller. (a) A four stages TFLN polarization controller. (b) Polarization splitter-rotator (PSR) and polarization rotator combiner (PRC). (c) 2×2 multimode interference (MMI) coupler. (d) One phase shifter and the corresponding trajectory on Poincaré sphere. (e) Combination of one phase shifter and two MMIs and the corresponding trajectory on Poincaré sphere.

implemented for the local oscillator (LO) in self-coherent transmission systems [22], [23], [24]. However, TFLN based polarization controllers for PM-IM/DD systems have not yet been demonstrated.

In this paper, we extend our work in OFC 2025 [25] and include more details on the proposed PM-IM/DD transmission scheme based on TFLN polarization controller and pilot-tone-assisted calibration-free polarization tracking algorithm. We present a detailed description of the fabrication process and key device characteristics. In addition, more experimental investigations were carried out. To achieve fast polarization control, we designed and fabricated a 4-stages MZI based polarization controller on the TFLN platform. The V_π of the fabricated TFLN based polarization controller is measured to be 3 V. The response time was 2 ns. The frequencies of pilots are optimized to be 2 MHz and 5 MHz for X polarization and Y polarization, respectively. Optimization of the pilot frequency and the pilot-to-signal power ratio (PSPR) was carried out. An optimal PSPR of -15 dB was obtained. Finally, we successfully demonstrated a 224 Gbit/s PM-PAM4 signal transmitted over 2 km of fiber with a polarization scrambling speed of 2 krad/s, which to the best of our knowledge, is a record polarization tracking speed for PM-IM/DD system. Our work has laid the foundation for the practical implementation of high-speed, low-complexity polarization demultiplexing for PM-IM/DD systems, paving the way for future advancements in optical interconnects for data centers and short-reach communication networks.

The remainder of this paper is organized as follows. In section II, we present the design concept and key parameters of the fabricated TFLN-based optical polarization controller. Section III introduces the pilot tone-based polarization tracking method specifically for PM-IM/DD systems. Section IV describes the experimental setup and provides detailed results to validate the proposed scheme. Finally, the paper is concluded in Section V.

II. Principle and Fabrication of TFLN Based Optical Polarization Controller

The polarization controller is based on a cascaded MZI architecture. Fig. 1(a) shows the schematic of our four-stages TFLN polarization controller, which consists of polarization splitter-rotator (PSR), polarization rotator-combiner (PRC), 2×2 multimode interference (MMI) couplers and phase shifters. Since only the transverse electric (TE) mode can propagate in the waveguide, as illustrated in Fig. 1(b), a PSR is used to convert the transverse magnetic (TM) mode of the incident light into the TE mode after polarization splitting for polarization insensitive operation. Conversely, the PRC performs the reverse operation, converting the TE mode back into the TM mode. The Jones matrix of an ideal 2×2 MMI, as shown in Fig. 1(c), is given by

$$\mathbf{M}_{\mathrm{MMI}} = \frac{1}{\sqrt{2}} \begin{bmatrix} 1 & j \\ j & 1 \end{bmatrix}, \tag{1}$$

the phase shifter introduces a phase difference between orthogonal polarization components and the Jones matrix of an ideal phase shifter, as shown in Fig. 1(d), is given by

$$\mathbf{M}_{\mathrm{Ideal\ PS}} = \begin{bmatrix} e^{j\theta_1} & 0 \\ 0 & 1 \end{bmatrix}, \tag{2}$$

by properly cascading MMIs with a phase shifter, various functional polarization modules can be realized. Two examples are shown in Fig. 1(d) and Fig. 1(e). The function of these two modules can be interpreted by observing the polarization state on the Poincaré sphere described by the normalized Stokes vector

$$\vec{S} = (S_1, S_2, S_3),$$

for example, assuming an input polarization state of $(0, 1, 0)$ (linear polarization at 45°). By sweeping the phase difference θ_1 in the first module (Fig. 1(d)), the resulting state of polarization (SOP) traces a trajectory on the Poincaré sphere along

which S_1 remains constant. The second module, including one phase shifter and two 3-dB MMIs as shown in Fig. 1(e), can be modeled as [26]

$$\mathbf{M}_{\mathrm{MMI+PS}} = je^{j\theta_1/2}\begin{bmatrix}\sin(\theta_1/2) & \cos(\theta_1/2)\\ \cos(\theta_1/2) & -\sin(\theta_1/2)\end{bmatrix}, \quad (3)$$

in this case, sweeping θ_1 results in a Poincaré sphere trajectory with S_3 constant. These two modules are used to better understand the principles of polarization control. It is theoretically feasible to use a pair of control phase values for a two stages polarization controller to transform an arbitrary input polarization state into a desired target polarization, such as the state corresponding to the Stokes vector $(0, 1, 0)$. However, due to limited tuning range of each unit, this minimal configuration imposes considerable control stress on individual stage. To alleviate this constraint, additional stages can be introduced to distribute the adjustment load across the system, thereby enhancing overall control performance. Nevertheless, increasing the number of stages inevitably leads to higher insertion loss, resulting in a trade-off between control flexibility and loss.

The overall transfer matrix of the polarization controller can be expressed as cascade phase shifters and four MMI couplers as shown in Eq. (4),

$$\begin{aligned}\mathbf{M}_{\mathrm{total}} = \mathbf{M}_{\mathrm{MMI}} \cdot \mathbf{M}_{\theta_4} \cdot \mathbf{M}_{\mathrm{MMI}} \cdot \mathbf{M}_{\theta_3} \\ \cdot \mathbf{M}_{\mathrm{MMI}} \cdot \mathbf{M}_{\theta_2} \cdot \mathbf{M}_{\mathrm{MMI}} \cdot \mathbf{M}_{\theta_1},\end{aligned} \quad (4)$$

where the phase shifter matrices are defined as

$$\mathbf{M}_{\theta_i} = \begin{bmatrix}e^{j\theta_i} & 0\\ 0 & 1\end{bmatrix}, \quad i = 1, \ldots, 4 \quad (5)$$

and the 3-dB MMI coupler is given by

$$\mathbf{M}_{\mathrm{MMI}} = \frac{1}{\sqrt{2}}\begin{bmatrix}1 & j\\ j & 1\end{bmatrix}. \quad (6)$$

Finally, the relationship between the input and output Jones vectors can be expressed as

$$\begin{bmatrix}E_x'\\ E_y'\end{bmatrix} = \mathbf{M}_{\mathrm{total}} \cdot \begin{bmatrix}E_x\\ E_y\end{bmatrix}, \quad (7)$$

which can achieve arbitrary output polarization with any input polarization.

The whole device is designed and fabricated on a commercial X-cut LN-on-insulator (LNOI) wafer (NanoLN) with a 400-nm thick TFLN layer, a 500-μm thick silicon substrate layer, and a 3-μm thick buried oxide (BOX) layer. The fabrication process starts with the TFLN structure patterning using an electron beam lithography system (Raith VOYAGER) on a 300-nm thick resist (ma-N 2403). Then, a 200-nm thick LN layer is removed using inductively coupled plasma reactive ion etching (ICP-RIE), followed by a deposition of 700-nm oxide over-cladding using plasma-enhanced chemical vapor deposition (PECVD). Finally, 1.1-μm Au metal electrodes are deposited using electron-beam evaporation and lift-off processes. The designed TFLN waveguide has a ridge height of 200 nm, a slab height of 200 nm, and a width of 1.6 μm. The edge couplers feature a polarization-dependent loss (PDL)

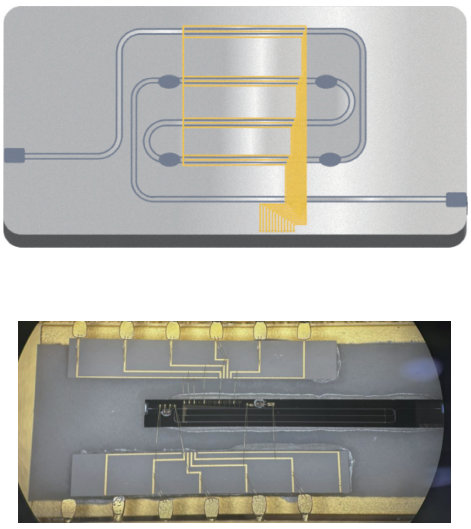

Fig. 2. TFLN polarization controller. (a) Schematic layout. (b) Packaged TFLN polarization controller.

of <1 dB, an optical bandwidth of >100 nm, and a coupling loss of <2 dB [27]. The PSR has a measured insertion loss of <0.5 dB [28]. The dynamic polarization controller device has an on-chip loss of less than 2 dB and a footprint of 1.8 cm × 4 mm [23]. Fig. 2(a) shows the schematic of TFLN based polarization controller. Fig. 2(b) shows the photo of the fabricated TFLN polarization controller inside a package box.

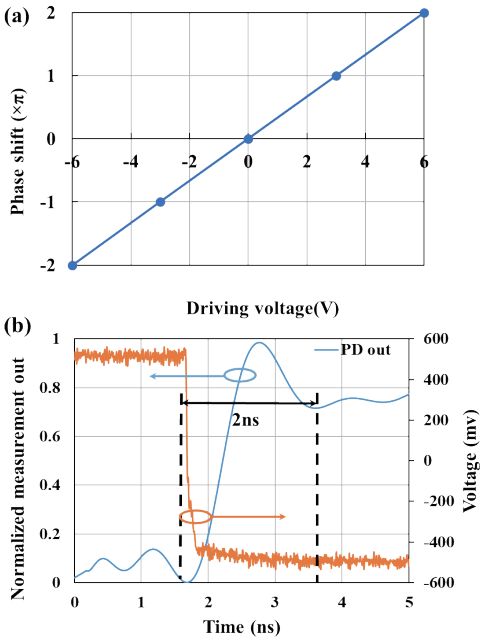

Fig. 3. (a) V_π measurement. (b) Response time measurement.

Fig. 3 shows the characterization results of the fabricated TFLN polarization controller. Fig. 3(a) shows the phase shift vs driving voltage. It can be seen that the V_π of the controller is 3 V. With a control voltage of ±12 V, the device was able to

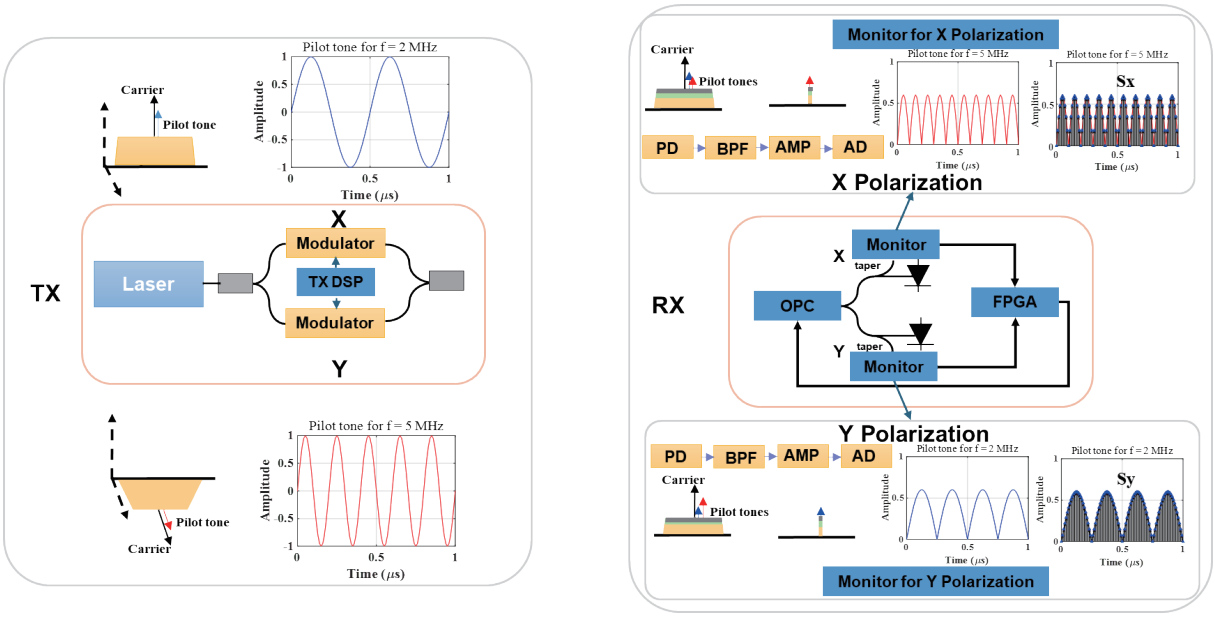

Fig. 4. Principle of proposed pilot tone based polarization trakcing scheme.

cover a range of $\pm 4\pi$. The response time of chip was measured by applying a square pulse with sharp rising edge and the results are shown in Fig. 3(b), indicating a fast response time of 2 ns was obtained.

III. Pilot-Tone-Based Polarization Tracking for PM-IM/DD Systems

In self-coherent systems, the SOP of LO can be tracked by monitoring the power difference between X and Y polarization components [23], [24]. However, this method cannot be directly applied to PM-IM/DD systems because the signals are modulated on each polarization. To achieve polarization tracking for PM-IM/DD signal, a pilot-tone based calibration free polarization tracking scheme is proposed in this paper.

Fig. 4 shows the principle of proposed pilot-tone based polarization tracking scheme. At the transmitter side, the pilot tones are generated and embedded into signal in digital domain prior to optical modulation. Pilot tones with different frequencies are assigned to X and Y polarizations, so that we can distinguish X and Y polarizations based on frequency of pilot tone at the receiver side. Since the frequency of the pilot tone is low (< 15 MHz), there would not be a significant impact on the transmission performance. The pilot tones can be described as

$$S_{x(y)}(t) = \sqrt{2} \cdot \sin(2\pi f_{x(y)} t) \cdot \sqrt{P_{\text{sig}} \cdot 10^{\text{PSPR}/10}}, \quad (8)$$

where f is the pilot tone frequency, and PSPR denotes the Pilot-to-Signal Power Ratio (in dB). Assuming the unscaled sinusoidal pilot has an average power of 0.5, the scaling ensures that the final pilot power achieves the desired PSPR relative to the signal power P_{sig}. The optimization for frequency and PSPR of pilot tone will be discussed in Section IV.

On the receiver side, the separated X/Y component was split into two parts: one for polarization tracking and the other for signal demodulation. In polarization tracking path, a low speed photo-diode (PD) with a bandwidth of 200 MHz converts optical signal into electrical signal. The embedded pilot tones are extracted via electrical band pass filters (BPFs), amplified, and then digitized using an analog-to-digital converter (ADC). The digitized pilot signals are then processed in an FPGA to generate feedback control signal to TFLN polarization controller for real-time polarization tracking.

Unlike previous approaches in [12], [13], [14], which require prior calibration to establish a voltage-to-phase response map, we introduce a calibration-free algorithm based on the power of pilot tones to achieve fast, simple and reliable polarization tracking. The core idea is iteratively adjusting the voltage applied to each stage of TFLN phase shifters based on the gradient direction inferred from pilot-tone amplitude. This enables effectively tracking polarization state without any prior knowledge of the phase-voltage relationship.

Initially, all four control voltages V_1, V_2, V_3, V_4 for the four stages of the phase shifters are set to zero. We denote the amplitude of the unwanted pilot tone (leaked from the undesired polarization) as P. At each iteration, a small perturbation ΔV is added to each voltage V_i one at a time, while the others are fixed. Considering the trade-off between computation complexity and tracking precision requirement in PM-IM/DD systems, the step size ΔV was set to correspond to a phase shift of $\frac{1}{64}\pi$. In each iteration, the pilot tone amplitude is measured and the gradient of each voltage

$$P_i = \frac{\partial P}{\partial V_i}, \quad i = 1, 2, 3, 4 \quad (9)$$

form a gradient vector $\{P_1, P_2, P_3, P_4\}$. The voltage vector is then updated according to the direction of the gradient to minimize the amplitude of the unwanted pilot tone. A leakage factor α is introduced to ensure stable operation and avoid

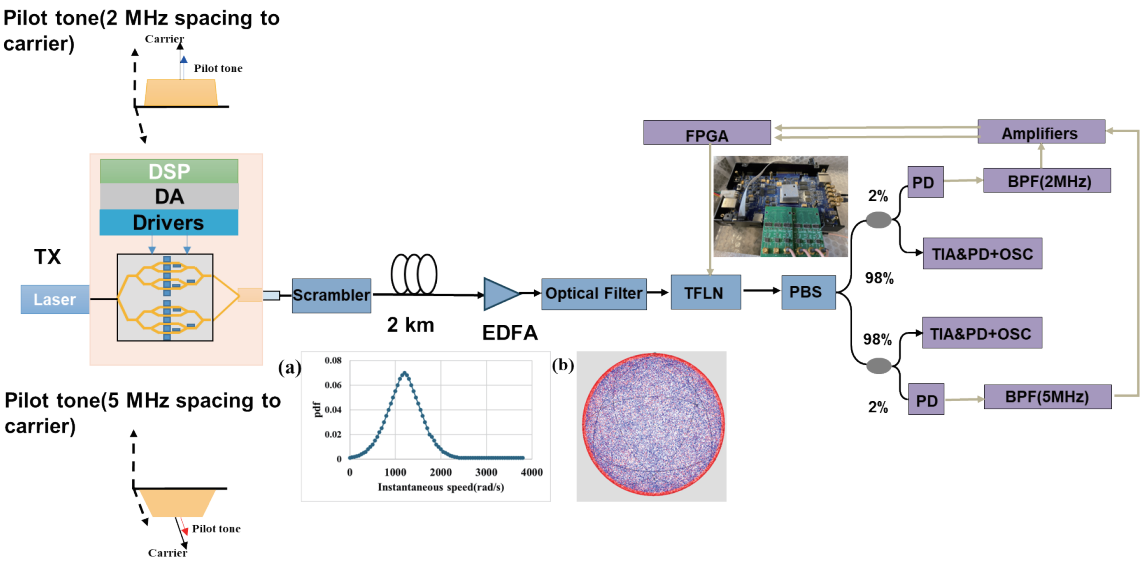

Fig. 5. Experimental setup of a 224 Gb/s polarization-multiplexed PAM4 (PM-PAM4) IM/DD transmission system. (a) Probability density function of the instantaneous SOP speed under a scrambling rate of 2 krad/s. (b) Stokes space trajectory corresponding to scrambling speed of 2 krad/s.

resetting. The voltage update is given by

$$V_i^{\text{new}} = \alpha V_i^{\text{old}} - \frac{P \cdot P_i}{P_1^2 + P_2^2 + P_3^2 + P_4^2}, \quad i = 1, 2, 3, 4 \quad (10)$$

where α is set to 0.99, and i denotes the stage index of optical polarization controller (OPC).

A feedback loop is repeated continuously to adapt to polarization variations in real time. Notably, this method eliminates the need for any phase-voltage calibration and is robust against environmental fluctuations. The overall flow of the tracking algorithm is summarized in Algorithm 1.

Algorithm 1 Pilot-Tone-Based Calibration Free Polarization Tracking Using TFLN polarization controller

Require: Initial voltage vector $\{V_1, V_2, V_3, V_4\} = \{0, 0, 0, 0\}$, voltage step size ΔV, leakage factor α, pilot tone power P

Ensure: Updated voltage vector $\{V_1^{\text{new}}, V_2^{\text{new}}, V_3^{\text{new}}, V_4^{\text{new}}\}$ applied to TFLN polarization controller

1: Measure initial pilot tone power P
2: **for** $i = 1$ to 4 **do**
3: Temporarily perturb voltage V_i by ΔV while keeping others fixed
4: Apply $\{V_1, ..., V_i + \Delta V, ..., V_4\}$ to the TFLN polarization controller
5: Measure resulting pilot tone power
6: Calculate normalized gradient direction:$P_i = \partial P / \partial V_i$
7: **end for**
8: Have $\mathbf{P}, \{P_1, P_2, P_3, P_4\}$, $\{V_1, V_2, V_3, V_4\}$
9: Update voltage vector according to:

$$V_i^{\text{new}} = \alpha V_i^{\text{old}} - \frac{P \cdot P_i}{P_1^2 + P_2^2 + P_3^2 + P_4^2}$$

10: Apply $\{V_1^{\text{new}}, V_2^{\text{new}}, V_3^{\text{new}}, V_4^{\text{new}}\}$ to the TFLN polarization controller

IV. Experimental Setup and Results

Fig. 5 illustrates the experimental setup of a 224 Gb/s PM-PAM4 IM/DD transmission system incorporating the proposed TFLN-based polarization controller. Due to the unavailability of a dedicated dual-polarization intensity modulator, a dual-polarization IQ modulator (Fujitsu FTM7992HM) with a 3 dB bandwidth of 35 GHz and a V_π of 4.2 V was repurposed to function as a dual polarization intensity modulator for the generation of a 2×56 Gbaud PM-PAM4 signal with embedded pilot tones. The center wavelength is 1550.42 nm. A polarization scrambler (LUNA PSY-201) was placed after the modulator for polarization scrambling.

Fig. 5(a) shows the probability density function of the instantaneous SOP speed under a scrambling rate of 2 krad/s, derived from the Stokes domain data presented in Fig. 5(b), as shown in the distribution, the instantaneous SOP speed exhibits a spread that can reach up to 2 krad/s. An erbium doped fiber amplifier (EDFA) was used to compensate for the large coupling loss from fiber to TFLN chip due to imperfect packaging process. According to [29], a coupling loss of 1.06 dB per facet can be achieved for TFLN chip. TFLN chip with proper packaging and therefore EDFA can be removed for the proposed PM-IM/DD transmission system in practice.

The transmitted PM-PAM4 optical signal was launched into the TFLN based polarization de-multiplexing after passing an optical band-pass filter. At the output of active polarization control chip, a polarization beam splitter (PBS) separates the orthogonal polarization components. Optical coupler with 98:2 split ratio was used to separate optical signal into two components. 2% of the optical signal is used for pilot tone extraction for polarization tracking. A low-speed photo-diode (PD) with a bandwidth of 200 MHz converts the optical signal into the electrical signal. The embedded pilot tones were extracted by using electrical 12th order Butterworth band-pass filters (BPF) with center frequency of 2 MHz and 5 MHz,

respectively. The bandwidth of both BPFs is 2 MHz. The filtered pilot tones are then amplified and digitized using an analog-to-digital converter (ADC) operating at 200 MSa/s. The digitized pilot signals are then processed in an FPGA (Xilinx Zynq-7000 series) to generate feedback control signal to TFLN polarization controller for real-time polarization tracking. The remaining 98% of signal is detected with a high-speed PD and sampled by a 160 GSa/s real-time scope for data recovery. The offline digital signal processing includes normalization, re-sampling, digital square and filtering based timing recovery, a 51 taps feed-forward equalization (FFE) based on decision directed least mean square (LMS) algorithm, symbol decision and BER calculation.

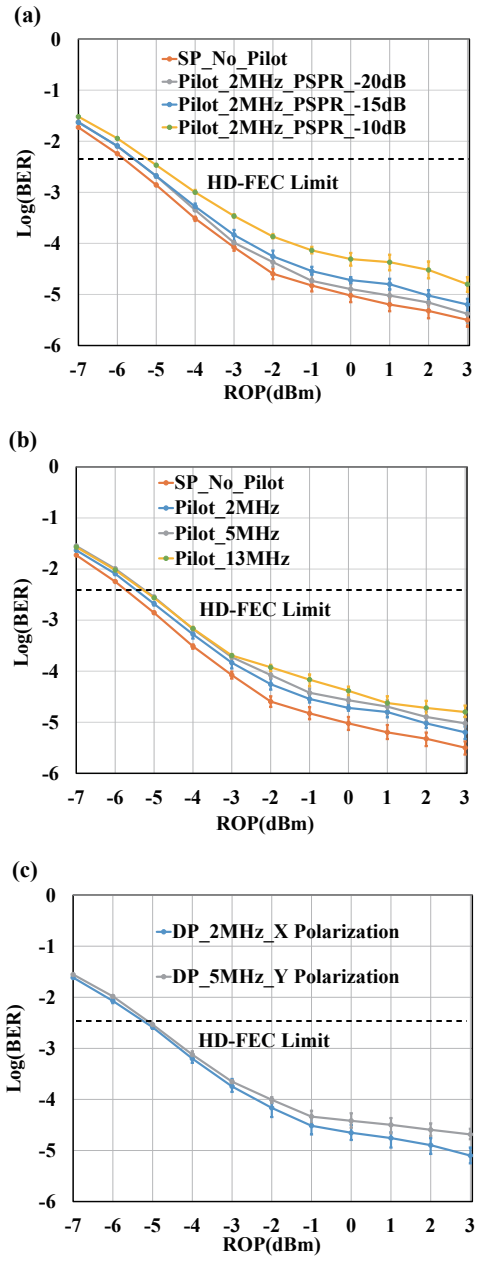

Fig. 6. Pilot tone parameter study. (a) Influence of PSPR. (b) Influence of pilot frequency. (c) ROP vs BER performance under X and Y polarization.

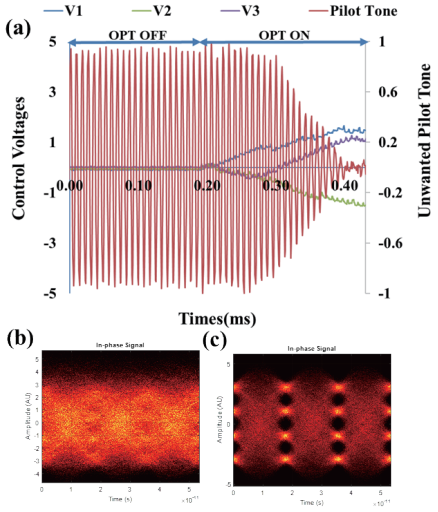

Fig. 7. (a) Polarization convergence speed. (b) The signal eye diagram when optical polarization tracking is OFF. (c) The signal eye diagram when optical polarization tracking is ON.

The pilot tone plays a vital role in polarization tracking by serving as a low-frequency reference embedded in the transmitted optical signal. However, the introduction of pilot-tone signal inherently impacts system performance. Therefore, we have carried out experimental study on the impact of two key parameters, which are PSPR and pilot-tone frequency. Fig. 6(a) shows the relationship between received optical power (ROP) and BER with different PSPRs. At the hard-decision forward error correction (HD-FEC) threshold of 3.8×10^{-3}, the measured receiver sensitivities for cases without a pilot and with a PSPRs of –20 dB, –15 dB, and –10 dB are –5.70 dBm, –5.45 dBm, –5.43 dBm, and –5.12 dBm, respectively. It can be seen that the penalty increases along with the increase of PSPR. However, if the PSPR is too low to be extracted from the signal, it will impact polarization tracking and system performance. Considering the trade-off between polarization tracking performance and BER performance, a PSPR of -15 dB was chosen for following experiment. We note that further improvements in pilot detection circuit, such as employing an electrical amplifier with lower noise and larger gain, it would be feasible to adopt even lower PSPR. Fig. 6(b) shows the experimental ROP vs BER for different pilot frequencies with a fixed PSPR of -15dB. At the HD-FEC threshold of 3.8×10^{-3}, the measured receiver sensitivities for cases without a pilot and with pilot frequencies of 2 MHz, 5 MHz, and 13 MHz are -5.66 dBm, -5.40 dBm, -5.22 dBm, and -5.16 dBm, respectively. It can be seen that penalty increases along with the increase in frequency of pilot tone. Finally, we choose pilot frequencies of 2 MHz for X polarization and 5 MHz for Y polarization in our transmission experiment.With PSPR optimized at -15 dB and pilot tone frequencies optimized 2(5) MHz. Fig. 6(c) shows the relationship between ROP and BER for a 224 Gbit/s PM-PAM4 back-to-back transmission system. At the HD-FEC threshold of 3.8×10^{-3}, the receiver sensitivities are -5.17

dBm for X polarization and -5.04 dBm for Y polarization, respectively.

Fast convergence is another key performance indicator for polarization tracking scheme, since it will enable fast link recovery from unstable state. Fig. 7(a) shows the evolution of unwanted pilot tone signal and control voltages through the transition from no optical polarization tracking to turning it on. It can be seen that from the time when optical polarization tracking is on, FPGA-based controller dynamically updates the control voltages for polarization control. The amplitude of unwanted pilot tone signal starts to converge to near 0 after 0.2 ms, which is 50 times faster than that of 10 ms reported in [9]. Fig. 7(b) shows the received eye-diagram when optical polarization tracking is turned off. Severe polarization interference was demonstrated. In contrast, Fig. 7(c) shows the received eye-diagram when optical polarization tracking is turned on, indicating a clear and high quality eye-diagram can be obtained with the proposed polarization tracking.

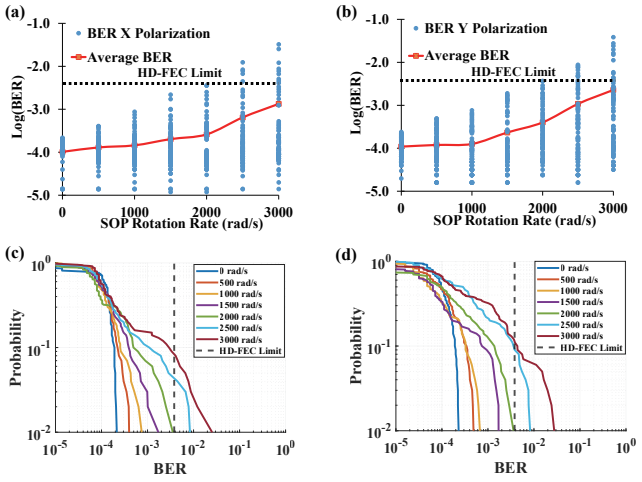

Fig. 8. Polarization tracking performance. (a) X polarization BER vs. scrambling rate with 2 MHz pilot tone. (b) Y polarization BER vs. scrambling rate with 5 MHz pilot tone. (c) CCDF curves of the BER for X polarization with different scrambling rates. (d) CCDF curves of the BER for Y polarization with different scrambling rates.

The BER performance after transmission with a received optical power of 2 dBm under different polarization scrambling speeds was measured and shown in Fig. 8. Fig. 8(a) shows the BER vs SOP scrambling rate for X polarization. Within 2 krad/s, all instant BER measurements are below the hard-decision forward error correction (HD-FEC) threshold of 3.8×10^{-3}. Although the average BER is below the HD-FEC threshold of 3.8×10^{-3} when scrambling rate is higher than 2 krad/s, there are few instant BER measurements higher than HD-FEC threshold. Fig. 8(b) shows the BER vs SOP scrambling rate for Y polarization. Within 2 krad/s, all instant BER measurements are below the hard-decision forward error correction (HD-FEC) threshold of 3.8×10^{-3}. Although the average BER is below the HD-FEC threshold of 3.8×10^{-3}. When scrambling rate is higher than 2 krad/s, there are few instant BER measurements higher than the threshold. Fig. 8(c) shows the complementary cumulative distribution function (CCDF) curves of the BER for the X-polarization under different scrambling rates. Fig. 8(d) shows the CCDF of Y polarization under different scrambling rates.

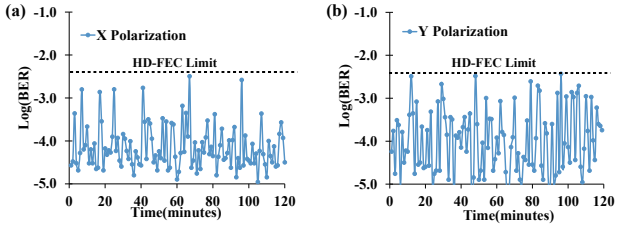

Fig. 9. Long Term BER stability test (2 krad/s scrambling, 60 s intervals, total 2 hours). (a) X polarization. (b) Y polarization.

Long term BER under 2 krad/s polarization scrambling rate was also measured to validate the stability of proposed optical polarization tracking scheme, as shown in Fig. 9. The BER was recorded every 60 seconds. Fig. 9(a) shows the BER performance over 2 hours for X polarization. All measurements are below HD-FEC threshold with an average BER of 1.91×10^{-4}. Fig. 9(b) shows the corresponding results for Y polarization, where all measurements remain below the HD-FEC threshold with an average BER of 3.80×10^{-4}. The results thus validate the long-term reliability of proposed optical polarization tracking scheme.

V. Conclusions

In this paper,we have demonstrated a PM-IM/DD transmission system by employing TFLN-based polarization controller integrated with pilot-tone based calibration free polarization tracking algorithm. Considering a HD-FEC threshold of 3.8×10^{-3}, a 224 Gbit/s PM-PAM4 signal is successfully transmitted and de-multiplexed with a polarization scrambling rate up to 2 krad/s. To the best of our knowledge, this is the record polarization tracking speed in PM-IM/DD transmission systems. The tracking speed can be further improved with FPGA operating at higher clock frequency, ADC/DAC with higher sampling speed and reducing the complexity of tracking algorithms, which will be topics of future research.This work proves the feasibility of TFLN based polarization controller for high-speed polarization tracking to enable low-cost PM-IM/DD solution for optical interconnects in data center applications.

References

[1] Cisco, "Cisco Annual Internet Report (2018–2023)," Cisco White Paper, Mar. 2020. [Online]. Available: https://www.cisco.com/c/en/us/solutions/executive-perspectives/annual-internet-report/index.html

[2] Nokia, "Network traffic in the zettabyte era: Through 2025," Nokia White Paper, Mar. 2021. [Online]. Available: https://onestore.nokia.com/asset/213660

[3] J. Mata *et al.*, "Artificial intelligence (AI) methods in optical networks: A comprehensive survey," *Opt. Switching Netw.*, vol. 28, pp. 43–57, 2018.

[4] C. Mavani, H. K. Mistry, R. Patel, A. Goswami, "Artificial intelligence (AI) based data center networking," *Int. J. Recent Innov. Trends Comput. Commun.*, vol. 12, no. 2, pp. 508–518, 2024.

[5] A. Uchiyama *et al.*, "Demonstration of 155 Gbaud PAM4 and PAM6 EML with narrow high-mesa EA modulator for 400 Gbps per lane transmission," in *Opt. Fiber Commun. Conf. (OFC)*,San Diego, USA, 2024, Paper Tu2D.1.

[6] L. Kulmer, T. Blatter, M. Kohli, Y. Horst, S.M. Koepfli, J. Leuthold, "Single carrier net 400 Gbit/s IM/DD over 400 m fiber enabled by plasmonic Mach–Zehnder modulator," in *Opt. Fiber Commun. Conf. (OFC)*, San Diego, USA, 2024, Paper W4H.5.

[7] X. Zhou, R. Urata, and H. Liu, "Beyond 1 Tb/s intra-data center interconnect technology: IM-DD or coherent?," *J. Lightwave Technol.*, vol. 38, no. 2, pp. 475–484, Jan. 2019.

[8] K. Kikuchi, "Fundamentals of coherent optical fiber communications," *J. Lightwave Technol.*, vol. 34, no. 1, pp. 157–179, Jan. 2016.

[9] A. Nespola *et al.*, "Real-time demonstration of polarization-multiplexed PAM using a compact silicon photonics device," in *Opt. Fiber Commun. Conf. (OFC)*, San Diego, USA, 2018, Paper Tu2C.6.

[10] A. Nespola *et al.*, "Proof of concept of polarization-multiplexed PAM using a compact Si-Ph device," *IEEE Photon. Technol. Lett.*, vol. 31, no. 1, pp. 62–65, Jan. 2019.

[11] D. W. U. Chan, D. Yi, Y. Tong, H. K. Tsang, "Towards 3.2 Tb/s direct detection polarization-multiplexed transceivers using on-chip microring-assisted coherent network," in *IET Conf. Proc. CP839*, Stevenage, UK, 2023, pp. 1314–1317.

[12] X. Wu, *et al.*, "Fully integrated dual-polarization silicon photonic transceiver with automated polarization control," in *Opt. Fiber Commun. Conf. (OFC)*, San Diego, 2023, Paper Tu2E.3.

[13] Y. Zhao, C. Doerr, F. G. Vanani, M. Takeshita, H. Kamisugi, "Dual-polarization IMDD system for data-center connectivity," in *Eur. Conf. Opt. Commun. (ECOC)*, Messe Frankfurt, Germany, 2024, Postdeadline Paper Th3A.5.

[14] Y. Zhao, C. Doerr, F. G. Vanani, M. Takeshita, H. Kamisugi, "Dual-polarization IMDD system for data-center connectivity," *J. Lightwave Technol.*, vol. 43, no. 2, pp. 456–462, Jan. 2025.

[15] Y. Zhao, C. Doerr, F. Liu, S. Mahadevan, F. G. Vanani, M. Takeshita, "425-Gbps/λ dual-polarization IM/DD transceiver," in *Opt. Fiber Commun. Conf. (OFC)*, San Francisco, USA, 2025, Paper Th4B.5.

[16] M. Bélanger and G. L. Yip, "Novel Ti:$LiNbO_3$ ridge waveguide linear-mode confinement modulator fabricated by reactive ion-beam etching," *J. Lightwave Technol.*, vol. 5, no. 5, pp. 1252–1257, May 1987.

[17] F. Heismann, "Analysis of a reset-free polarization controller for fast automatic polarization stabilization in fiber-optic transmission systems," *J. Lightwave Technol.*, vol. 12, no. 4, pp. 690–699, Apr. 2002.

[18] B. Koch, R. Noé, V. Mirvoda, D. Sandel, "140-krad/s, 254-gigaradian endless optical polarization tracking, independent of analyzed SOP," *IEEE Photon. Technol. Lett.*, vol. 29, no. 2, pp. 175–178, Jan. 2017.

[19] C. Wang *et al.*, "Integrated lithium niobate electro-optic modulators operating at CMOS-compatible voltages," *Nature*, vol. 562, no. 7725, pp. 101–104, Oct. 2018.

[20] M. Xu *et al.*, "High-performance coherent optical modulators based on thin-film lithium niobate platform," *Nat. Commun.*, vol. 11, no. 1, p. 3911, Aug. 2020.

[21] Y. Liu *et al.*, "Low V_π thin-film lithium niobate modulator fabricated with photolithography," *Opt. Express*, vol. 29, no. 5, pp. 6320–6329, Mar. 2021.

[22] Z. Lin *et al.*, "High-performance polarization management devices based on thin-film lithium niobate," *Light Sci. Appl.*, vol. 11, no. 1, p. 93, Apr. 2022.

[23] Z. Li *et al.*, "High-speed polarization tracking using thin film lithium niobate integrated dynamic polarization controller," *Opt. Express*, vol. 31, no. 24, pp. 39369–39378, Nov. 2023.

[24] W. Chen *et al.*, "600-krad/s polarization tracking using a DC-stable integrated polarization controller based on thin film lithium niobate," in *Eur. Conf. Opt. Commun. (ECOC)*, 2024, pp. 735–737.

[25] J. Cao *et al.*, "Experimental Demonstration of 224 Gbit/s PM-PAM4 IM/DD Transmission System using TFLN Polarization Controller," in *Opt. Fiber Commun. Conf. (OFC)*, San Diego, CA, USA, 2025, Paper W1E.5.

[26] X. Wang, Y. Zeng, R. Liao, J. Zhao, and J. Yu, "Reset-free adaptive polarization controller on a silicon-photonic platform for a self-coherent communication system," *Opt. Lett.*, vol. 48, no. 7, pp. 1546–1549, Apr. 2023.

[27] R. Gan *et al.*, "Fabrication tolerant and broadband polarization splitter-rotator based on adiabatic mode evolution on thin-film lithium niobate," *Opt. Lett.*, vol. 47, no. 19, pp. 5200–5203, 2022.

[28] B. Chen, Z. Ruan, M. Wang, S. Gong, and L. Liu, "High-performance and fabrication-tolerant edge coupler on thin film lithium niobate based on a three-dimensional inverse taper," *APL Photon.*, vol. 9, p. 116111, 2024.

[29] G. Chen, K. Chen, Z. Yu, and L. Liu, 'Low-loss and broadband polarization-diversity edge coupler on a thin-film lithium niobate platform," *Opt. Lett.*, vol. 48, pp. 4145–4148, 2023.